New insight on the risk profile pertaining to lithium-ion batteries under thermal runaway as affected by system modularity and subsequent oxidation regime

Arnaud Bordes, Guy Marlair, Aurélien Zantman, Sylvie Herreyre, Arnaud Papin, Philippe Desprez, Amandine Lecocq

New Insight on the Risk Profile Pertaining to Lithium-Ion Batteries Under Thermal Runaway as Affected by System Modularity and Subsequent Oxidation Regime

Arnaud Bordes[a], Guy Marlair*[a], Aurélien Zantman[a], Sylvie Herreyre[b], Arnaud Papin[a], Philippe Desprez[b,c] and Amandine Lecocq[a]

[a]*Institut National de l'Environnement Industriel et des Risques (Ineris), Parc Technologique Alata, BP2, 60550 Verneuil-en-Halatte, France*
[b]*SAFT, 111 bvd Alfred Daney, 33074 Bordeaux, France*
[c]*present address; ACC, Centre R&D – 136 quater Avenue d'Aquitaine, 33520 Bruges*

[*]*corresponding author: guy.marlair@ineris.fr*
Tel: +33 344556348 – Fax; +33 344556699

Abstract

It is now well established that lithium-ion battery technology is a key electrical energy storage device in the fight against the global warming, helping us to make transportation more sustainable and securing intermittent renewable energy sources. The requirement to keep the thermal runaway (TR) hazard under control is among remaining issues for continuous and sustainable use of lithium-ion batteries. This experimental work brings a new insight on the issue, by performing and analyzing of a series of NMC pouch cell internal short circuit tests reflecting progressively the overall level of integration of such cells when modularly assembled in sub-systems to constitute the full pack. While replicating always the same TR triggering procedure in these experiments, our heat, gas and particle emission analyses reveal that the consequences in terms of chemical (e.g. toxic and corrosive) and thermal threats arising from a default cell running into thermal runaway may greatly vary according of the level of integration mocked up during the abuse test. This work also shows that thermochemical reactions/combustion regimes and their transitions following TR (towards possible flaming combustion or simply ending-up by hot gas degassing) are among key determinants of the whole risk pattern.

Graphical abstract :

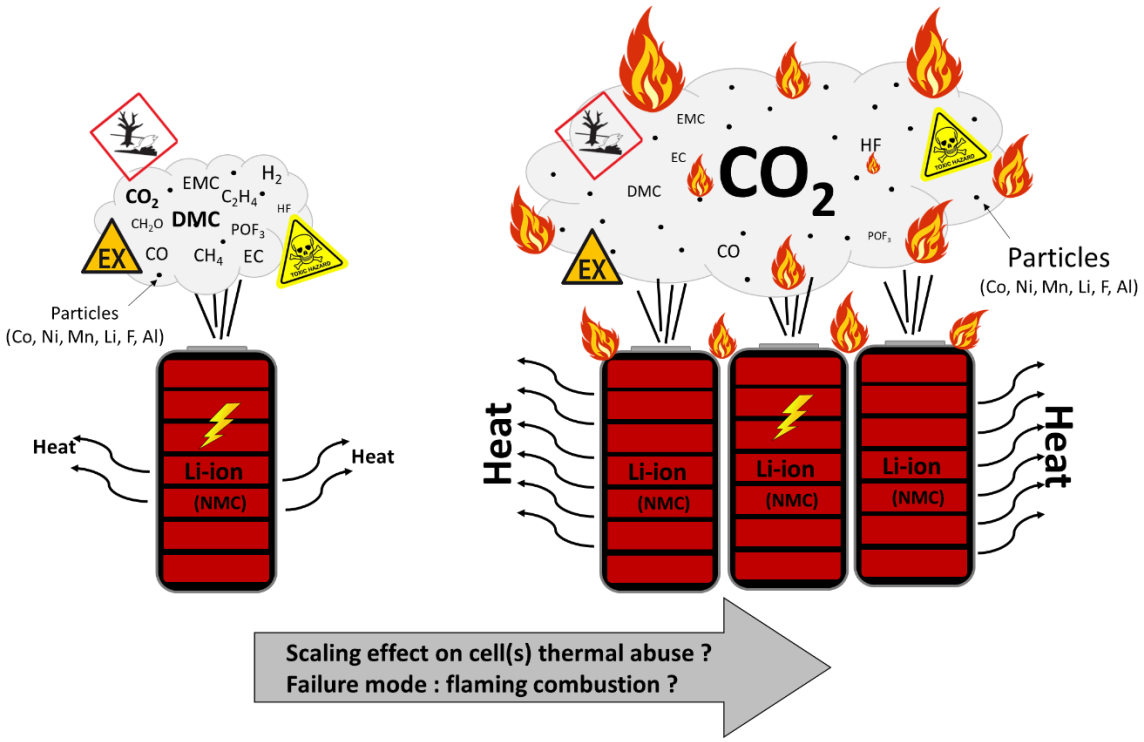

Keywords: Li-ion battery safety; thermal runaway propagation; level of test cell integration; combustion regime; gas analysis; particle emission

1. Introduction

Over the past years, Li-ion Batteries have become an energy storage device of choice and are currently powering many applications. Stakeholders are anticipating a short-term, rapid and sustainable growth of their usage, driven by various applications including large stationary electrical energy storage facilities and electric vehicles which are currently promoted by public policies around the world to fight against climate change[1]. This fast development has been possible thanks to the constant improvement of Li-ion performances in terms of specific energy

density and significant decrease in production cost. But one factor that should not be forgotten and that allowed Li-ion batteries system to be adopted, is their satisfactory safety level, regardless of their use. Safety management strategy of these batteries has to cope with short innovation timelines and may, fortunately, rely more and more on the progressive consolidation of safety-focused professional guidance[2], international standards (e.g. emitted by International Electrotechnical Commission TC21/SC21A, TC120 Committees, British Standard Institution Publicly Available Specification (PAS) 7060[3]) or regulations (United Nation (UN) R100[4], UN TDG[5], Directive 2006/66/EC and amending Regulation (European Union) No 2019/1020 …) aiming at putting LIBs safety under control on their full value chain[6,7]

As most energy storage systems, Li-ion battery systems present a risk in case of misuse, poor design or inadequate manufacturing. These mishaps can trigger a well-identified hazardous phenomenon known as battery thermal runaway (TR), subsequently leading to cascading adverse events like fires, release of intense heat, projection of battery debris and emission of toxic and explosive gas[8-10]. When the battery system is large enough, like battery packs of tens of kW range powering electric vehicles or battery subsystems in the MW/tens of MW range used for stationary storage applications, TR events can cause severe damage and have already proven to be dangerous in a number of recent incidents affecting first responders or surrounding persons. Examples of such events include the fire of a stationary storage container in Arizona in 2019 injuring two firefighters,[11,12] or a number of Electric Vehicle (EV) fires, occurring sometimes in underground parking lots[13]. An even more dramatic fire and explosion event happened in April 2021 in Beijing on a Battery Energy Storage System (BESS) complex integrating photovoltaic production system, grid integrated electric energy storage and connections to EV charging stations[14]. With the increasing use of batteries, we may anticipate that incidents involving batteries will rise at a constant rate. To define protection measures, mitigation means, first responders' tactics, and the best course of action in case of accident,

data about the hazards generated by these battery systems and about potential triggering factors are required. This task is particularly difficult because each battery system might reacts differently, depending on a number of parameters, starting with the cell chemistry used (both anode, cathode and electrolyte)[15-17], the state of charge (SOC) at the moment of the incident[18-20] and the system architecture. The influence of these parameters is the subject of several studies. As pressure for capacity performance increase is leading to cell integration with tighter timelines, building a solid know-how in this field is crucial. The integration level plays a critical role: the behaviour of a single cell and the same cell integrated into a module or a pack can be drastically different[21]. For a defined battery, the presence of sustained flaming combustion in case of thermal runaway is an outcome very difficult to predict, as it is inconsistent from one abuse test to another. The thermochemical process associated with the thermal runaway event, leading or not to flaming combustion can clearly modify the overall hazards produced by a battery[22]. Therefore, in this study, the focus is put on the relation between the consequences of thermal runaway of a battery sample in regard with the regimes of thermal decomposition /oxidation occurring. In other word, it will sort out the cases ending up -or not- to ignition and flaming combustion. The quantity and type of gas released, the heat generation, and particles emissions, are measured in order to compare the dangerous nature of each scenario.

To study the influence of the scenario on the outcome of a battery thermal runaway, cell and module level thermal runaways are triggered on different samples made out of the same cells. To initiate a thermal runaway representative of real-life situation and without affecting the cell integrity due to test fit-for purpose modification, or by adding extra energy to the system, an internal short circuit is created using an internal heater. Tests are run on automotive type cell, cluster of cells and module in conformity with the modular cell assembly configurations of battery packs found in automotive industry. This study is part of the Europe-

funded project *DEMOBASE*[23-25], that is aiming to develop seamless and safe integration of Li-ion batteries in electric vehicles.

2. Materials and methods

2.1 Tested samples

Cell type test sample

$LiNi_{1/3}Mn_{1/3}Co_{1/3}O_2$ (NMC 111)/graphite flat pouch prototype cells of a capacity of 19 Ah, nominal energy of 70 Wh corresponding to a specific energy of 145 Wh/kg and of dimensions 220x177x10 mm were assembled at SAFT (Bordeaux-France). A prototype cell is composed of 31% positive electrode active materials and additives, 17% negative electrode active materials and additives, 18% current collectors, 23% electrolyte, 4% separator and 7% of remaining compounds as packaging materials and connectors, for a total mass of 485.3 ±0.3 g.

Cluster scale test sample

A cluster assembled by IFEVS was composed of 3 pouch prototype cells in parallel (3P configuration) separated by aluminium plates. The cluster contained a polymer compression pad on one face, and Acrylonitrile butadiene styrene (ABS) was used as holder component on negative and positive sides as illustrated in Figure 1 (white plastic visible on picture a and b). The assembly was maintained by steel plates on both sides using tie-rods. The central cell of the cluster was equipped with an internal heater. Nominal voltage and capacity of the cluster were 3.7 V and 57 Ah respectively.

Module scale test sample

A module assembled by IFEVS was composed of 3 clusters in series leading to a 3P3S configuration. Each cluster was separated by a polymer compression pad and an aluminium plate. The 3 clusters' assembly was maintained by steel plates on both sides using tie-rods as illustrated in Figure 1. The central cell of the central cluster was equipped with an internal heater. Nominal voltage and capacity of the module were 11 V and 57 Ah respectively.

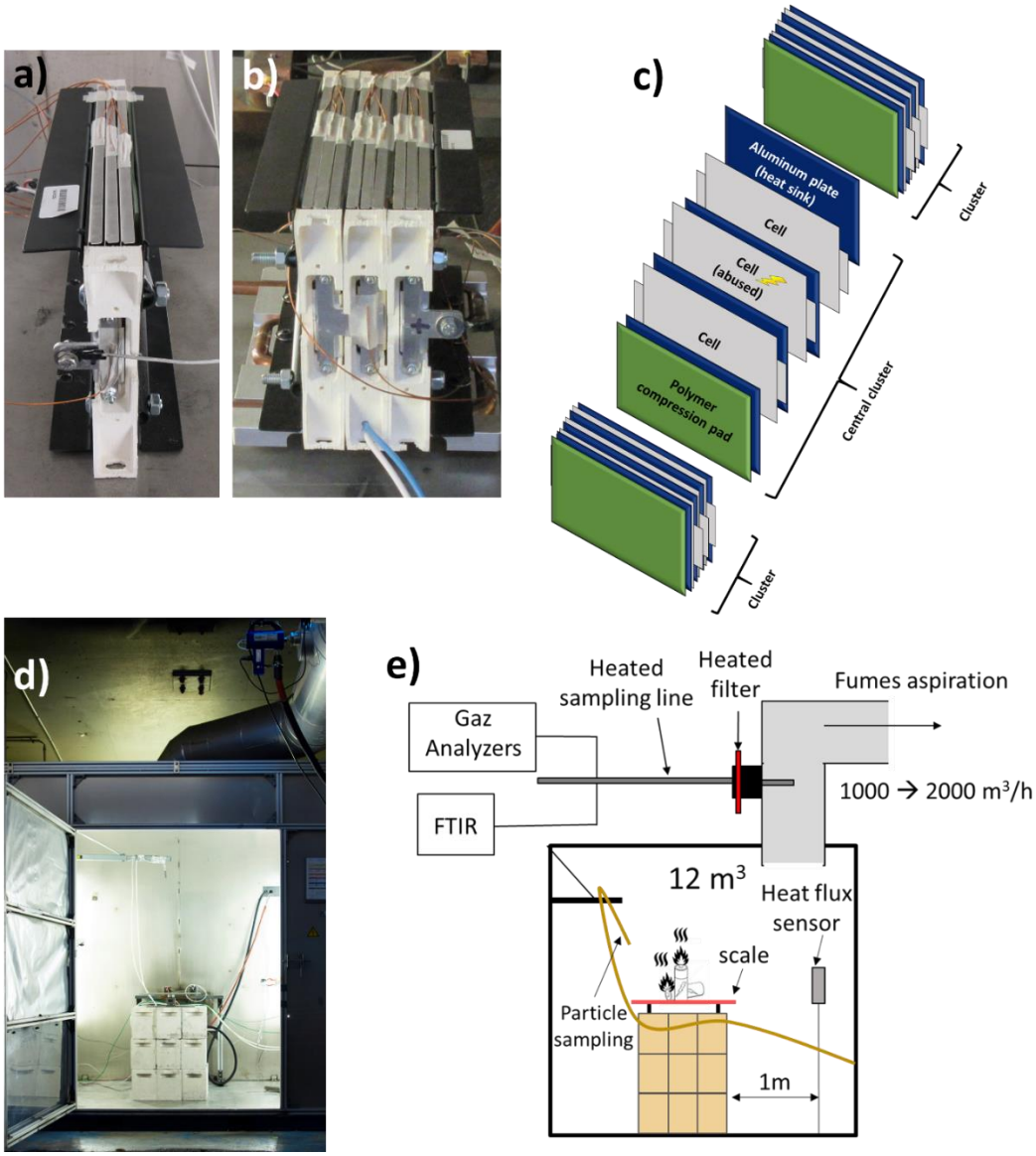

Figure 1 : a) Image of tested cluster composed of three pouch cells b) image of the tested module composed of 3 clusters (9 pouch cells) c) representation of the module assembly d) image of testing chamber in test configuration e) representation of the test set-up

2.2 Internal heater implementation

A specific pouch cell with an embedded internal heater was developed by SAFT. A picture of the heater is shown in figure 2. The heater consists of a 0.25 mm diameter Tungsten filament with a length of 10 cm that is twisted to form a 1.5 cm side square. The heater is put in contact with the negative electrode (center part, in the middle of the stack). Two specific tabs on the side of the cell allow the connection to an external power supply. The internal heater is activated by applying a current to heat the filament that creates a very localized internal defect and induces an internal short-circuit inside the cell leading to thermal runaway. Using this method, the extra energy transferred to the system by heating is minimal compared to conventional thermal abuse (external heater) leading to TR by overheating. According to Zhang *et al.*, the localized external heating method is simple to operate and ensures a good repeatability but it does not allow to control the internal short circuit type (active material-current collector, active material-active material…)[26].

2.3 Abuse tests set up and measurements

Abuse tests on cell, cluster and module levels are performed in a 12 m^3 test chamber equipped with a ventilation system remotely piloted to fully extract gases in the exhaust system connected to a gas scrubber system, which canalizes and cleans up gas and smoke emissions before rejecting them in the atmosphere. All tests are performed under air with a flow rate in the test chamber at approximately 1 000 m^3/h for cell abuse tests and 2000 m^3/h for cluster and module abuse tests.

The sample is positioned on a weighting platform in the centre of the test chamber as represented in Figure 1. Two heat flux sensors are positioned at about 1 m from the sample in the test chamber. Filters are positioned near the sample for particle sampling; analyses of Al,

Co, Cu, Li, P, Ni, Mn trapped in the PTFE filter are performed by inductively coupled plasma - optical emission spectrometry (ICP-OES) after mineralization using a mixture of hydrofluoric acid and nitric acid (HF, HNO_3) in a closed microwave oven according to the NF EN 14385 standard. Analysis of fluorinated species trapped in the cellulosic filters are performed by ionometry after extraction and alkali fusion of the filter according to the NF X 43-304 french standard.

Online gas sampling is carried out through a heated line (180 °C) positioned on the extraction duct and connected to various analysers allowing real time monitoring and analysis of the gas stream. A non-dispersive infra-red analyser (NDIR) is used for CO_2 and CO, chemiluminescence-based on-line analyser is used for nitrogen oxides (NO_x). Additionally, on-line analysis of total hydrocarbons (THC) making use of flame ionization detector (FID), and mass spectrometry based analysis for H_2 are also performed. A Fourier-transform infra-red (FTIR) spectrometer (Thermo Scientific Nicolet 6700, gas cell of 2 m) for further analysis of gases and vapours of interest is also exploited. The online FTIR apparatus provides quantitative information regarding gas release from battery thermal runaway such as organic carbonates (EC, DMC, EMC, etc.), hydrocarbons (CH_4, C_2H_4, etc.), aldehydes (OCH_2, CH_3CHO, etc.), carbon oxides (CO_2, CO), fluorinated species as HF and POF_3, and other species as HCN, NO_x and SO_2 responding in the infra-red domain, according to adequate calibration processes. For pertinent exploitation of obtained FTIR spectra, characteristic wavenumber ranges for each component are selected with the aim of limiting interferences as much as possible. The gas analysis methods followed the principles of ISO 19702 standards[27]. According to our experience and ISO 19702, the gas measurement repeatability, taking into account sampling and analysing for this kind of measurement is in the range of 5-15% depending of the gas. For HF, despite the precautions taken to limit the loss of signal, due to its high reactivity, some of it may be lost in the sampling line and the filter leading to a possible additional underestimation.

The total effective heat of combustion and the fire growth are determined using the carbon dioxide generation (CDG) fire calorimetry technique[28,29] based on CO2 and CO flow rate. For this kind of fire and integrating the test levels, our estimation of the expectable heat release rate (HRR) accuracy lies within 15% to 20% based on our own long-term experience in such type of measurements[30] for the CDG calculations. These values are consistent with similar fire calorimetry techniques, where the burning fire load is largely unknown or variable in time[31]. In addition to this intrinsic precision, in the case of battery fire, heat loss due to electrical (joule heating) or chemical process (salt and other inorganic components exothermic decomposition decomposition) cannot be accounted for in the calculation based on CO_x species production, and might represent up to 1/3 of the total thermal energy released[32]

A heat flux meter is positioned at about 1 m from the sample in the test chamber. A video recording is performed throughout the test in order to observe visually cascading effects. A video compilation of the main events is available in the supplementary information.

Abuse test at cell level corresponds to an internal short circuit (ISC) test. The test consists in applying a current profile to the internal heater embedded in the pouch cell up to thermal runaway onset. The cell is placed horizontally inside a support composed of two insulated plates on either side of the cell and metal plates in contact with insulated plates as illustrated in figure 2. The assembly was maintained by four spacer bars with flanges. This support was designed to mock-up the integration of the cell inside a module employed in the electric vehicle. A central groove is created in one of the insulated plates on the side in contact with the cell in order to position one thermocouple to measure the temperature at the surface of the cell during the whole duration of the internal short-circuit test. Four additional thermocouples are positioned at around 2 cm from each side of the pouch cell to measure the temperature of emitted gases. During the test, cell voltage is recorded.

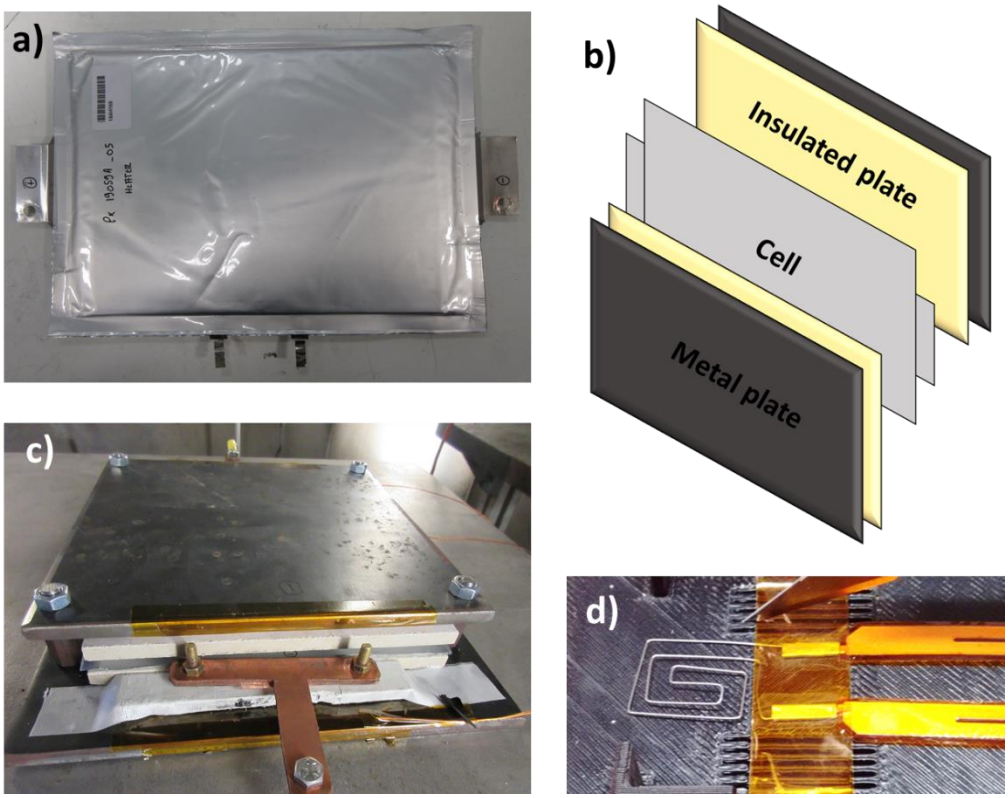

Figure 2 : a) Image of the instrumented tested cell (tabs of the internal heater are visible) b) representation of the cell test set-up assembly c) Image of the cell test set-up d) image of the internal heater

Abuse test on cluster and module levels consist in triggering an internal short circuit in the central cell with the same procedure used at cell level, with the aim to assess thermal runaway propagation. Thermocouples are distributed over the whole cluster surface and on negative and positive connectors as well as for the module. Cluster and module voltages are recorded during the tests.

Prior to the abuse tests, cell, cluster and module are fully charged at C/5 with a potentiostat (Biologic, Claix, France), less than 12 hours before conducting the internal short-circuit tests.

3. Results and discussion

3.1 Experimental results overview

Figure 3 presents the thermocouples positioning and the main events that occur during the cell level internal short circuit test. Thermocouple 1 is placed on the surface of the cell at this center whereas thermocouples 2, 3, 4 and five are placed nearby in order to record temperature of vented gases. 20 seconds after the activation of the internal heater, the cell enters in thermal runaway. Its voltage drops suddenly from 4.2 V (full charge) to 0 V. In the meantime, the temperature recorded at one external edge of the cell increases abruptly from ambient temperature to 410 °C, corresponding to a gas venting event. The temperature on the cell surface increases as well but at a lower rate and to lower temperature illustrating that the main failure mode of this thermal runaway scenario is a degassing of the cell without significant combustion with flames. The video of the test is available in supporting information and the main events are extracted and presented in figure 3 b, c, d and e. This observation confirms that the thermal runaway results mainly in gas emission. The fumes are black in the beginning and white smoke appears after a few seconds. A brief inflammation of the emitted gas is visible in figure 3 e, appearing at a distance from the cell. The induced flaming combustion is very brief and accounts for only a small part of the emitted gas.

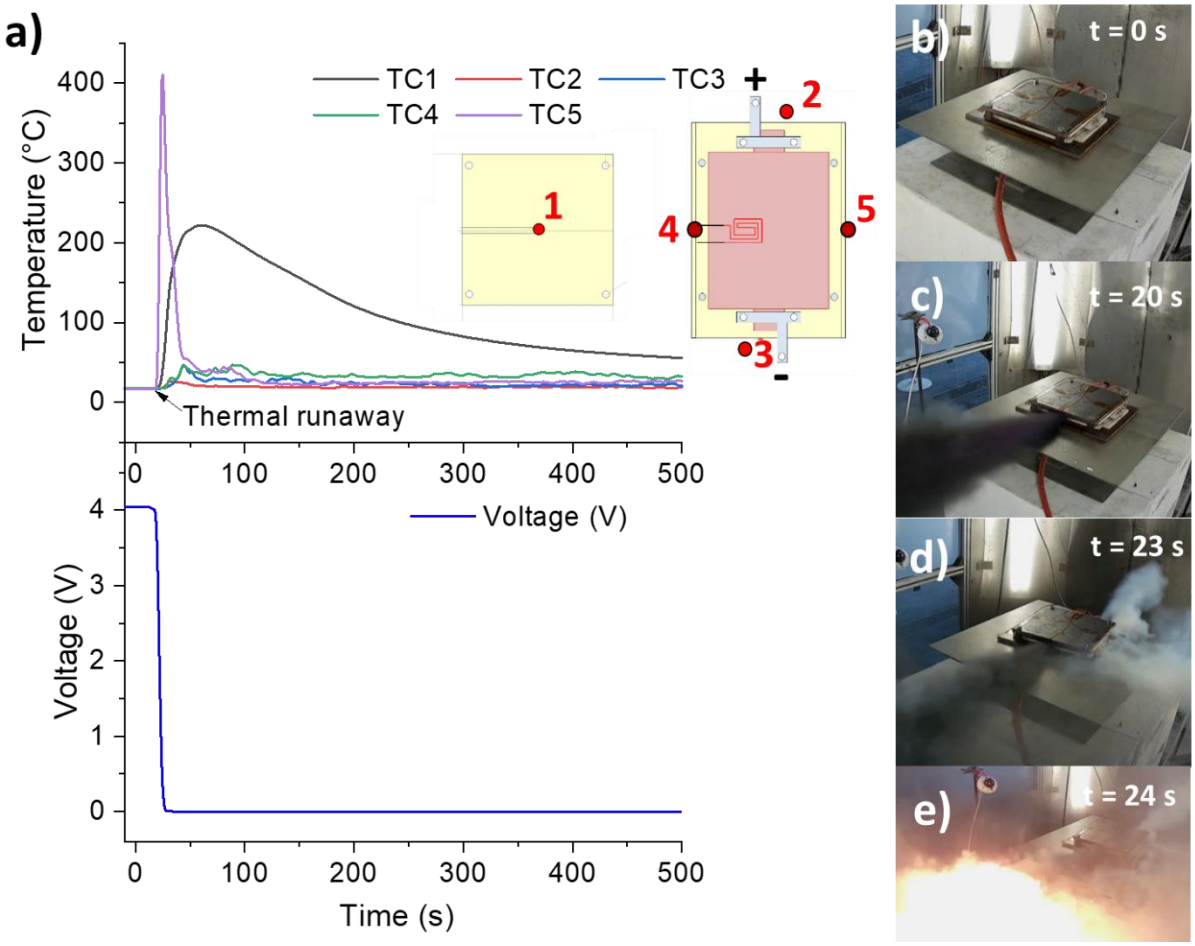

Figure 3 : a) Temperature and voltage as a function of time recorded during cell level internal short-circuit test. Position of the thermocouple and heater is detailed in the inset schema. b) cell in test configuration before abuse c) first fume emission (20 s after heating) d) fume emission development, white fumes appear e) very brief inflammation of gas. Full video is available in supporting information.

The internal short circuit test is then reproduced at cluster scale. Main results are presented in figure 4. Only main events are reported and, the full test video is available in supporting information data. After 20 seconds of heating, an important swelling of the cell abused (central cell) is observed. This swelling is likely caused by gas accumulation inside the pouch cells. 3 seconds after the beginning of the swelling, an important emission of white smoke is observed (figure 4b) and a maximal temperature of 265 °C is registered on the edge of the cell. The voltage of the cluster remains steady due to the parallel architecture of the

cluster and it is observed that only one cell has reacted. Once the reaction is almost over, a small and very brief flaming combustion process is taking place. The fume emission almost stops and 110 seconds after the 1st cell reaction, the cluster voltage drops to 0 V and the second cell enters in thermal runaway. This cascading thermal runaway is characterized by a maximal temperature of around 600 °C and significant flame development (figure 4c). The flames rapidly fade but never stop, probably due to a sustained combustion that is being maintained by plastic components of the cluster. The voltage drop is probably the result of the electric signal loss due to the impact of flaming combustion which only occurred after the second cell thermal runaway onset. 3 minutes after the 2nd cell reaction, the third and last cell of the cluster enters in thermal runaway, leading to further fire intensification and fumes emission with a maximal temperature close to 800 °C (figure 4d). Due to the proximity of thermocouples 1, 2 and 3 (around 1 cm), the cell swelling and fumes/flame random orientation, the temperatures recorded by thermocouples cannot be directly correlated to the cell they were originally placed on, but give a general information about nearby temperatures.

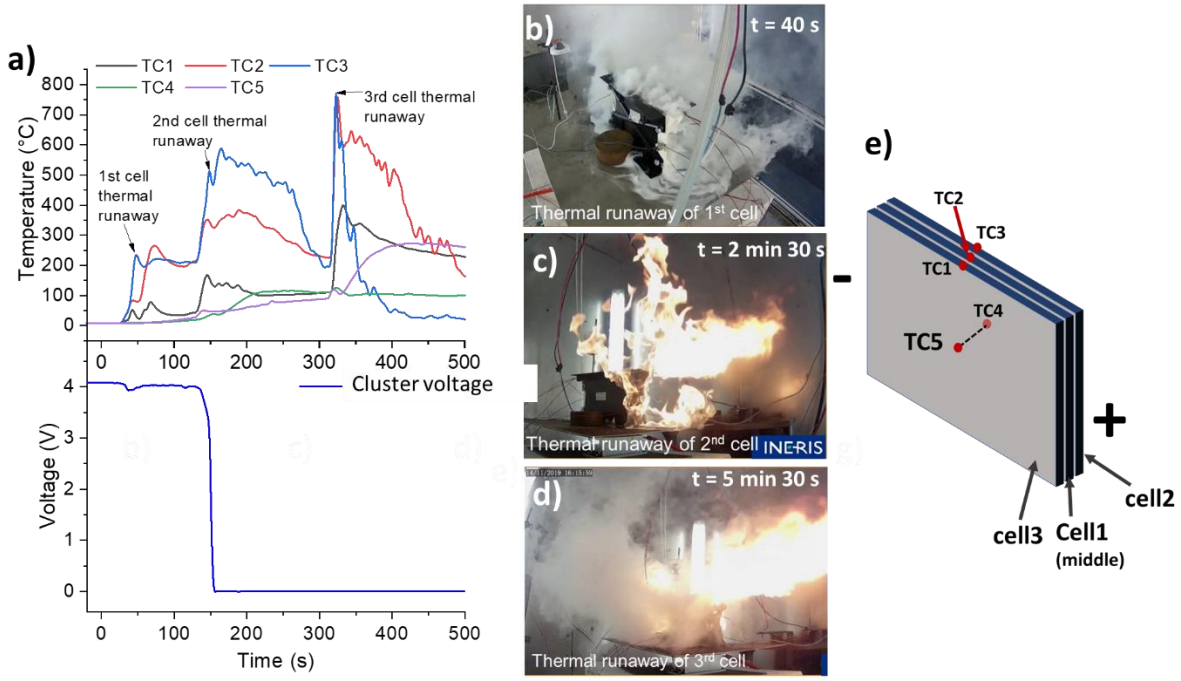

Figure 4: a) Temperature and voltage as a function of time recorded during cluster level internal short-circuit test. b) first fume emission (40 s after heating) corresponding to central cell thermal runaway c) flaming combustion process corresponding to 2nd cell thermal runaway d) flaming combustion process corresponding to 3rd cell thermal runaway. e) cell numeration and thermocouple position. Full video is available in supporting information.

After cell and cluster level, the whole module thermal runaway test is performed, again setting internal short circuit of a single cell as triggering method. The results are shown in figure 5. Reactions are similar to the one observed at cluster level. At first time, the abused cell swells (visible on the video) and releases a large amount of fumes (figure 5 b). The reaction then slows down for 60 seconds before a more violent reaction occurs, corresponding to the simultaneous reaction of the two adjacent cells, producing strong flames as shown in figure 5c and resulting in a voltage drop to 0 V. Contrary to the cluster level, both adjacent cells react at the same time. Neighboring clusters are affected by the reaction only with a moderate increase in temperature, not sufficient to induce a thermal runaway of their cells. The protection barrier offered by the polymer/aluminum cluster separators appears effective in avoiding cascading propagation from

one cluster to another. Small flames corresponding to plastics slow combustion are observed almost 25 min after the first cell reactions. Those flames are visible on the video in supplementary information.

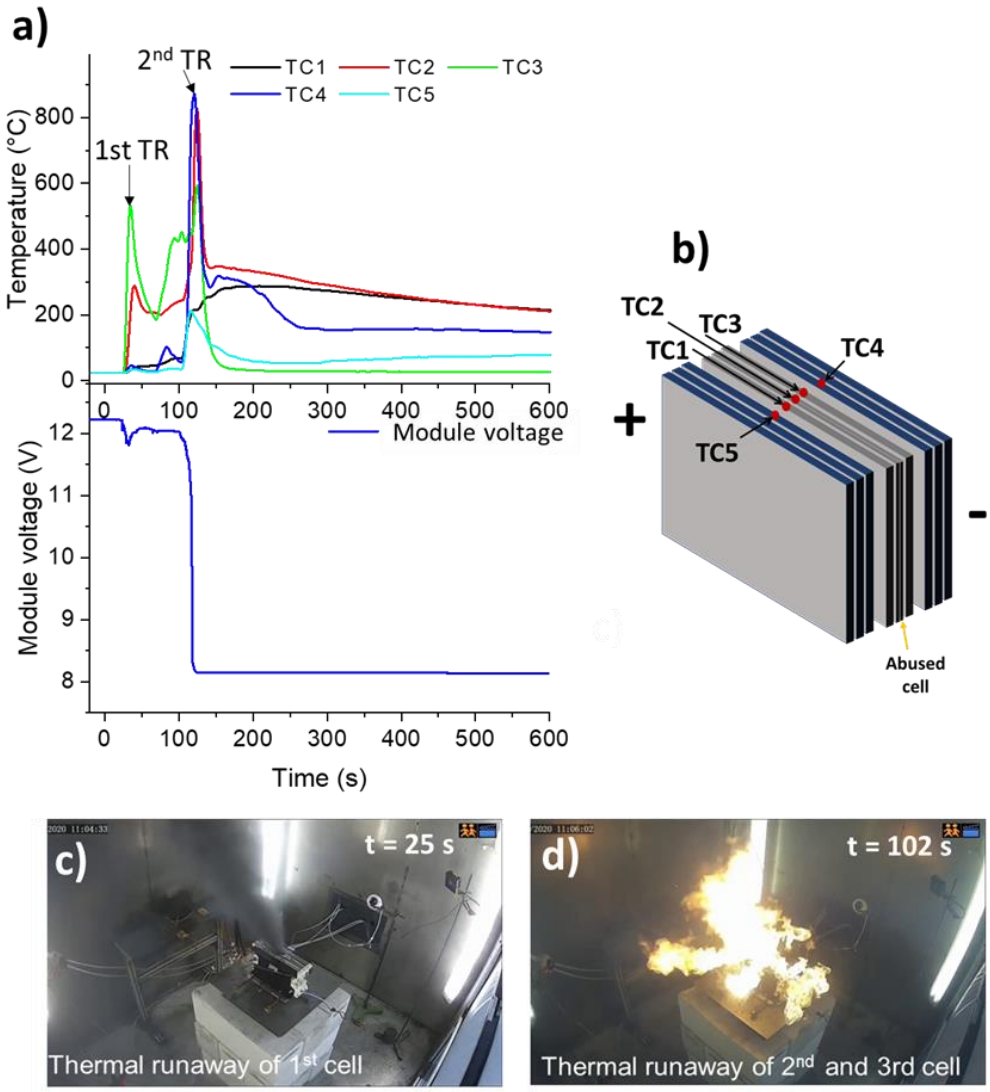

Figure 5 : a) Temperature and voltage as a function of time recorded during module level internal short-circuit test. Position of the thermocouple is detailed in the inset picture. b) thermocouples positioning c) first fume emission (25 s after heating) corresponding to central cell thermal runaway d) flaming combustion process corresponding to 2nd and 3rd cells thermal runaway. Full video is available in supporting information.

3.2 Gas emissions

During all the tests, online gas analysis is performed, to measure the quantity and analyze the composition of the gas mix released during each test. Table 1 summarizes the gas emission quantification results. Identified species are, among others, carbon oxides ($CO + CO_2$) released from combustion process[33], organic carbonates originating from electrolyte evaporation and species like H_2, CH_4, C_2H_4, CH_2O, POF_3 and HF coming from decomposition processes of various components[34-36].

At cell level, last line of table 1 allows to see that the total amount of gas measured is close to 38 L (0.5 L/Wh or 78 L/kg) and almost half of it consists of carbonates. The amount quantified is lower than the scarce emission results found in the literature for NMC chemistry (200 L/kg[37] 780 L/kg[15]). Nonetheless, differences in test set ups, abuse methods and failure modes (ARC tests and fire exposure tests) can explain this inconsistency.

In comparison with the tests run at cluster and module levels, the total volume of gas is much lower, showing that gas emissions are not directly proportional to the number of cell present in the system. At cluster level, this quantity is close to 350 L (1.7 L/Wh). At module level, the quantity of gas released is 466 L corresponding to 0.8 L/Wh. The last value may be misleading in terms of reflecting maximum expected degassing from worst case scenario at module level, since only three cells out of nine composing the module took part in the reaction (limited propagation). Taking into account only the energy of the cells that participated to the reaction, a corrected relative gas emission amount would be around 2.2 L/Wh, close to the one observed at cluster level.

The differences observed between single cell level and assembly of cells are mainly due to the large production of CO_2 related to the important combustion step made visible in the latter scenarios by the presence of flames for the cluster and module case studies. CO_2 emission is not the only gas emitted in varying quantities between the three tests and the overall trend

observed is that test scale level (cell/cluster/module) influences the nature of gas emission in lithium battery abuse tests.

	Quantity of gas measured during ISC test								
	Cell level			Cluster level			Module Level		
	g	L	mL/Wh	g	L	mL/Wh	g	L	mL/Wh[1]
CO_2	25.1	12.8	183	587.4	299	1420	808.5	411	1950
CO	5.4	4.3	61	23	18.4	87	14.2	11.4	54
HF	0.07	0.1	1	1.4	1.6	8	3.4	3.8	18
POF_3	1.4	0.3	4	1.3	0.3	1.3	1.12	0.2	0.9
H_2	0.1	1.3	19	0.9	10.9	52	nm	nm	nm
CH_2O	0.3	0.2	3	0.2	0.1	0.5	0.5	0.4	2
CH_4	0.7	1	14	2.0	2.9	14	1.5	2.2	10
C_2H_4	0.7	0.5	7	1.3	1	5	1.2	0.9	4
DMC	40.3	10	143	36.1	7.8	37	96.2	23.9	113
EMC	15.5	3.3	47	13.4	3.3	16	40.0	8.6	41
EC	14.8	3.8	54	12.4	3.2	15	13.5	3.4	16
NOx	nd	nd	nd	1.2	0.9	4	0.5	0.4	2
Total	104	37.7	539	680	349	1662	980	466	2210

Table 1 : quantity of gas measured during internal short-circuit tests - Cluster level = 3 cells Module level =9 cells. The measurement of H2 failed during test at module level. [1] At module level, only cells taking part to the reactions were taken to account. The total is obtained by summing contribution of each species.

In order to better understand the influence of thermal runaway scenario on the resulting effects, and especially the influence of fire development in the gas emission, the test at cluster level can be studied in more detail. Figure 6 shows the gas emission as a function of time during this test.

Three clear series of peaks are visible, corresponding to the reactions of the three cells. As previously presented (figure 4) the reaction of the first cell results in fume without fire and the reaction of the second and third cells emits flames.

When the flames start, depending on the species, two kinds of behavior can be identified:

1- gaseous species produced in larger quantities after the flame appearance. It is the case of CO_2 (x8); HF (x10) and NO_x (x4).

2- gaseous species produced in smaller quantities after the flame appearance as witnessed for CH_4 (/12), C_2H_4 (/7), CO (/10), POF_3 (/4), carbonates (/7), CH_2O (almost disappearing) and H_2 (almost disappearing).

The dramatic increase in CO_2 amounts is driven by the advanced combustion. The ratio CO/CO_2 (vol.) is close to 0.01 in the presence of flame showing a good combustion, not limited by the O_2 availability[38]. On the contrary, in the first phase, when only fumes are visible, the CO/CO_2 ratio is close to 0.8, illustrating a dominant pyrolytic process[39]. O_2 is nevertheless emitted and might be attributed to several sources like organic carbonates and cathode material decomposition.

The increase in HF production, linked to the emergence of flames, can be explained by different factors, the main one being temperature increase that favors fluorinated compounds thermal decomposition. Another one is that combustion reaction produces water that enters in the HF reactions mechanism promoting HF formation but, in the meantime, water can also condensate aqueous HF and diminish its presence in the gaseous phase.

POF_3 presence is rarely reported in the literature and the parameters influencing its formation seem complex. Solchenbach and coworkers have evidenced the possible emission of POF_3 from $LIPF_6$ thermal decomposition by CG/MS under wet argon gas flow[40]. In regards of this study and the results presented by Larson *et al.*[35], it seems that less violent reaction (no high temperature, lower Heat Release Rate (HRR),…) favors the presence (or persistence) of this reactive intermediate. In our case, it is most likely that during the second phase of the reaction it reacted with water to form HF, explaining POF_3 decrease and HF increase[41].

Easily flammable species like H_2, organic carbonates, methane (CH_4), ethylene (C_2H_4), fuel the combustion reaction and their emissions therefore dramatically decrease during the 2nd

and 3rd cells reactions where the combustion is almost complete. The emission of formaldehyde (OCH_2); one of the components coming from linear carbonates reduction[42], observed in the fumes of the 1st thermal runaway cell disappeared during the fire phase.

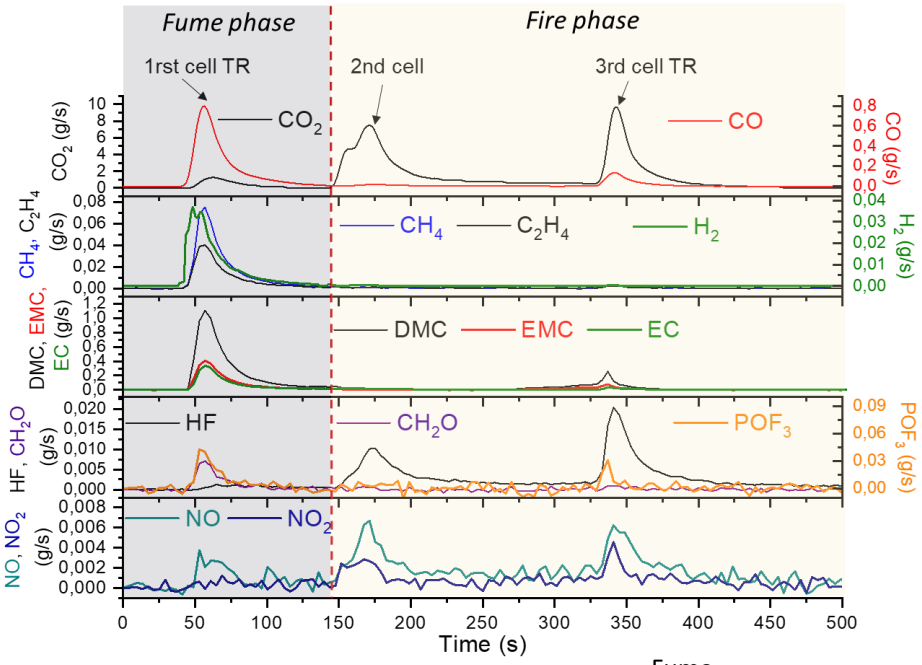

	Quantity of gas measured during cluster ISC test (mg/Wh)	
	1st cell (no fire)	2nd and 3rd cell (fire)*
CO_2	520	3936
CO	273	28
HF	1	9,6
POF_3	11	2,9
H_2	13	0,2
CH_2O	2,1	0,1
CH_4	25	2
C_2H_4	15	2
DMC	404	56
EMC	149	21
EC	120	29
NOx	2,1	7,9
Total	1520	4094

** cumulative values*

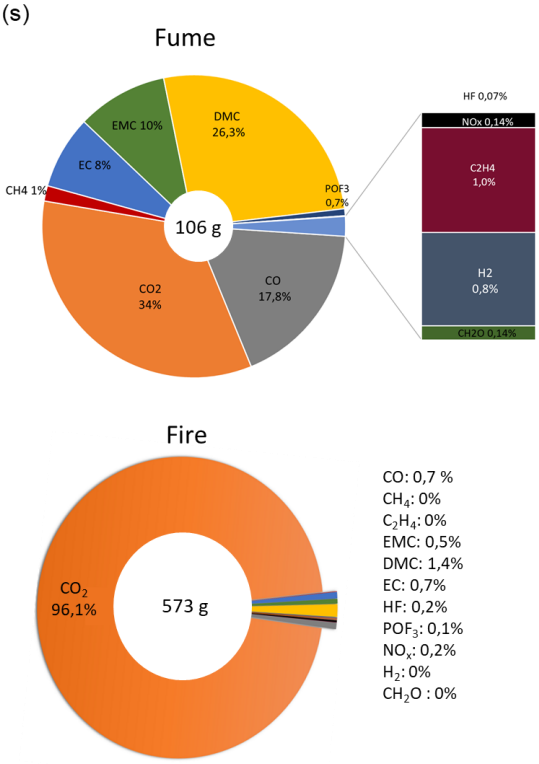

Figure 6 : Cluster level internal short-circuit gas release. The cluster reaction is divided in two phases: "fume phase" (grey part) corresponding to reaction of first cell and

fire phase (yellow part) corresponding to reaction of 2nd and 3rd cells. Based on this separation, the table present gas quantities emitted during each phase. Pie charts express mass percentages of the different compounds found in the gas mix and presented in the adjacent table.

The occurrence of flaming combustion is not the only factor influencing gas emission. The scale of the test itself clearly plays a role. NO_x formation is indeed inexistent at cell level (see Table 1) but is detected at cluster and module level. This phenomenon is attributed to the presence of ABS plastic in the assembly, the only significant source of N-fuel in the battery assembly capable of releasing NOx in our test conditions[43]. Indeed, this component revealed to be partially burnt at the end of the test as visible on the video in supplementary information. It is also known that emissions of NOx in fire conditions are due to dominating fuel-N process by opposition of thermal NOx and prompt NOx emission routes, which require the involvement of a combustible material containing the nitrogen element in its chemical structure[44]. Of course, the combustion promotes the plastic burning and thus the NO_x emissions.

3.3 Particle emission

In addition to gas analysis, the emission of inorganic particles is studied during these tests. Mass of particles presented in figure 7 corresponds to the quantity collected for analyses in the same conditions for the three tests, and does not represent the total quantity emitted. This amount is almost two orders of magnitude higher in case of cluster and module test when flames were emitted. Although, particulate sampling and capture processing used does not allow for formal analysis of relating emission kinetics and evolution over time, the increase in particle emission can be certainly attributed to the flaming combustion phase activation. Particle emissions are also visible in the videos presented in supplementary information, which again supports this hypothesis.

In contrast to the quantitative aspect, the nature of the emitted particles is similar in the three tests and does not seem affected by the scale or the scenario of the thermal runaway. Ni,

Mn and Co are the main species, coming from the positive electrode (NMC 111). Ni content in the particulate flow is overrepresented compared to its theoretical proportion in the cell chemistry. Li, P and F mainly come from the electrolyte salt ($LiPF_6$). Li is also found in the positive and negative electrodes once cycled. F can come from the binder (PVdF) or additives present in the electrolyte. Al from the positive electrode is present in relatively low quantity (between 6% and 9%) whereas only traces of Cu are detected. The thermal stability of Cu (melting point of 1085 °C), much higher than Al (melting point of 660 °C) might explain this difference in particle emission. Available studies are limited and do not allow to capture a clear tendency in term of metallic particulate emissions.[45]

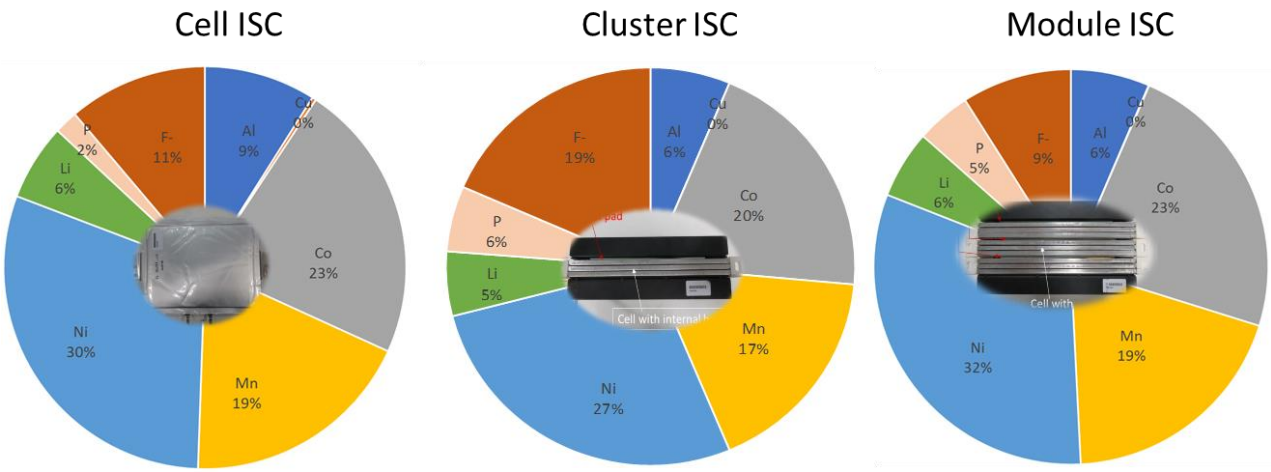

Figure 7 : particles emission during internal short circuit tests at cell, cluster and module level

3.4 Thermal effects

From thermochemistry laws, it is easy to evidence that the heat released in a complete combustion exothermic process involving carbonaceous species is clearly related to oxygen consumed by oxido-reduction reaction as well as to carbon dioxide production. This is known right from the beginning of the combustion science development but this only from the early

80's that modern fire calorimetry using the main gas streams involved in combustion has been established and promoted nearly in every fire laboratory[46] in substitution to the sensible enthalpy rise method, by researchers such as Babrauskas, Parker and Janssens (Oxygen Consumption (OC) principle) or Tewarson and Marlair (Carbon Dioxide Generation (CDG) principle). Both methods have their own advantages and drawbacks. The application of these techniques is rather challenging in the case of Lithium-ion batteries, in particular due to the fact that this is an electrochemically active device. However the current practice for heat release evaluation in battery testing under thermal or electrical abuse conditions is predominantly applying these fire calorimetry laws, often without reporting about their limitation.[18,47].

In this study we have decided to select the CDG principle over the OC principle because of the specific nature of the object under consideration and the practical difficulty arising with OC due to oxygen release process potentially associated with the chemistry of the positive electrode material.

Based on this principle, figure 8a presents the evolution of heat of combustion over time for the three tests. As for gas and particle generation, the effective heat of combustion is not found proportional to the electrical energy stored or the number of cells taking part in the reaction, whilst the studied scenario and especially the ignition event play a crucial role in the overall thermal threat as reflected by the measured HRR. When no flaming combustion is taking place, the effective heat of combustion is comprised between 6 to 12 kJ/Wh, reflecting very incomplete combustion processes driven by semi-oxidative environment created in a first step with oxygen released by the cathodic transition metal oxide mix. In contrast, when flames are visible, the effective heat of combustion jumps to 50 kJ/Wh. Several factors explain this behavior:

1- Flaming combustion is a much more effective thermochemical process than semi-oxidative process during degassing phase without flames bound to semi-pyrolytic conditions prevailing in such conditions and releasing at least partially unburnt combustible gases and vapors

2- Flaming combustion triggers the involvement of other compounds that would not participate in the overall thermochemical reactions when ending up in cell degassing without ignition (plastics from the outside, separator…). Under these conditions, since more materials are burnt, more heat is produced

3- In the absence of outer flames, the combustion is incomplete because of lower oxygen availability (O_2 mostly available from internal material decomposition, see CO / CO_2 ratio analysis previously done), producing comparatively less heat.

As expected, this internal combustion without flaming combustion is not or barely detected by the heat flux sensors positioned at 1 m from the samples (recorded flux is presented on figure 8b) showing the limited amount of heat released. This sensor is positioned far enough from the sample to rely on heat flux radiation isotropic process and check consistency with heat release calculated by CDG. Due to flames fluctuations, quantitative values are nonetheless to be taken with precaution.

In addition to the heat flux recorded by the heat flux sensors, figure 8b allows to compare the heat release rate over time for the test at cluster and module levels. Even if in both cases only 3 cells took part in the reaction, and the total heat of combustion related to electrochemical components is similar, the kinetics of the reaction is different. At cluster level, three peaks are identifiable. A small one (20 kW), attributed to the reaction of the first cell with no flames, and two bigger ones (100-130 kW) related to the reaction of the two neighbor cells, in the presence of fire. At module level only two peaks are visible, a small one (25 kW) also associated with the reaction of the first cell with no flames, and a second large one (250 kW) due to the simultaneous reaction of the two adjacent cells. One explanation of this difference in the

thermal response behavior is the integration of the abused cell in a larger system, that at cluster level brings extra insulation to the adjacent cells, limiting heat loss and concentrating the reaction. Also, at the end of the reaction of the cells, plastics components of the module, present in larger amount than for cluster level, keep burning for almost 20 min, leading to an overall increase of 30% of the effective heat of combustion whereas the heat release rate remains very low in this final stage.

These differences, although not impacting the total effective heat of combustion attributed to electrochemical components, play an important part in the hazard presented by a battery system over time and should be considered when performing risk analysis for a given battery concept.

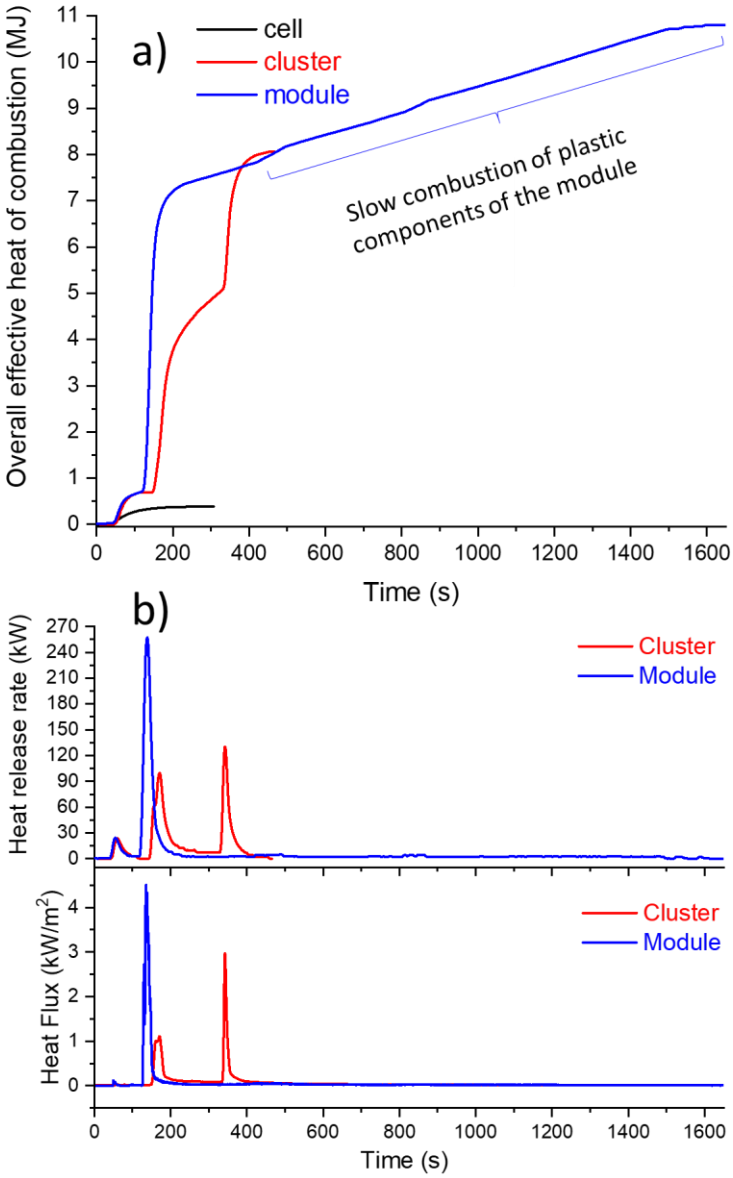

Figure 8: a) overall effective heat of combustion measured based on CDG principle during internal short circuit at cell, cluster and module level b) heat release rate measured based on CDG principle and heat flux measured by heat flux sensors during internal short circuit at cluster and module level

3.5 Considerations for the resulting risks

As evidenced in preceding subsections, the scale (i.e. level of abused cell integration) and the scenario (i.e. flaming or non flaming post runaway combustion process) play a crucial role in the outcome of the thermal runaway of a single cell. These outcomes will directly impact the

overall hazards produced by the battery in case of incident and should be thoroughly studied and considered before completing the design and integrating battery system in a given application.

Thermal hazard

First, the heat release behavior is significantly influenced by the occurrence of flaming combustion, producing further energy by fuel consumption in addition to exothermic decomposition reaction associated with the thermal runaway process. Without flames, the total heat released is lower and, most importantly, critical HRR is cut-off since only sensible enthalpy remains released in the environment in the absence of flames. This last statement is crucial because HRR intensity determines the potential propagation through external heat flux ignition to adjacent battery system components or buildings and a thermal flux higher than 2.5 kW/m^2 starts to be hazardous for humans under short time exposure. However, considering only the existence or absence of flaming combustion is not enough to fully evaluate the risk. The propagation is directly linked to heat transfer modes and thermal runaway reaction kinetics explaining that the actual level of cell integration significantly influences the HRR. We have shown that the propagation reaction kinetic might be different, resulting in higher HRR for large systems when several cells can react simultaneously. In addition, at higher level of assembly (module, pack, system), additional materials might bring additional combustible feedstock in a fire scenario, increasing the related HRR and the heat of combustion.

Toxic gas hazard

The evaluation of toxic gas hazard is crucial since it is key information requested by first responders before their intervention to ensure their safety. Moreover, in case of large incident it is important to have data on gas emissions to protect the surrounding populations and decide between partial precautionary evacuation or confinement[33]. The gas mix evolves greatly in the

presence of fire. First, the produced gas volume increases due to large emission of CO_2. Other components like HF, POF_3 or CO are produced in different amounts as detailed in figure 4.1. Considering this, the state-of-the-art fire-induced toxicity indexes related to given critical conditions, developed by ISO TC92 SC3 were used to propose a preliminary toxicity assessment. ISO 13571:2012 standard[48] is intended to address the consequences of human exposure to the life-threatening components of fire and can be used to estimate the time at which individuals may reach the incapacitation stage, a critical state requiring external rescue over self-evacuation of impacted population.

Long term effects are not considered. Because they are physiologically unrelated, and mechanistically independent, asphyxiant and irritant toxicants are treated as separate critical indices in the latest version of ISO 13571. By using data from figure 6 obtained at cluster level, we can compare the asphyxiating and irritating levels of the gas mix in terms of critical indices in case of fumes emission with and without fire.

Fractional effective doses (X_{FED}) are computed to consider additive effects of most asphyxiant pollutants (e.g. CO, HCN...) taking dose effect into account. It can be obtained from the evolution of pollutant concentrations in a given enclosure using the following equation (1):

$$X_{FED} = \sum_{t_1}^{t_2} \frac{[CO]}{35000} \Delta t + \sum_{t_1}^{t_2} \frac{[HCN]^{2.36}}{1.2 \times 10^6} \Delta t \quad (1)$$

The terms containing [CO] and [HCN] in equation (1) at each time increment are to be multiplied by a frequency factor V_{CO2} (equation 2) to account for the increased rate of asphyxiant uptake due to hyperventilation.

$$V_{CO2} = \exp\left(\frac{[\%CO_2]}{5} \right) \quad (2)$$

During the tests of our study, HCN was not detected; therefore, X_{FED} profile is only driven by the production of CO. X_{FED} value is significantly higher in case of fumes emission without fire, as compared to fire owing to the fact that the production of CO is significantly higher in this case.

The second index for toxicity assessment of ISO 13571:2012 standard is the fractional effective concentration (X_{FEC}) considering additive effects of essentially irritant fire gases (e.g. inorganic acids...) and taking into account their irritant effect. It can be obtained using the following equation (3):

$$X_{FEC} = \frac{[HCl]}{F_{HCl}} + \frac{[HBr]}{F_{HBr}} + \frac{[HF]}{F_{HF}} + \frac{[SO_2]}{F_{SO_2}} + \frac{[NO_2]}{F_{NO_2}} + \frac{[acrolein]}{F_{acrolein}} + \frac{[formaldehyde]}{F_{formaldehyde}} + \sum \frac{[irritant]}{F_{C_i}} \quad (3)$$

where F_i is the critical concentration of each irritant gas that is expected to seriously compromise occupants' tenability.

No exposure limit was found for POF_3 but we may assume that the toxicity of POF_3 acts through other poisoning mechanisms than HF by comparison with chlorine analog $POCl_3$/HCl and critical limits of exposure might be lower for POF_3 than for HF. However, without consolidated exposure limit for POF_3, we considered a reasonably conservative hypothesis that the critical concentration of POF_3 was equivalent to that of HF (i.e. 500 ppm), as it was done in a previous study[42].

In our study, whereas X_{FEC} profile in case of degassing without flaming combustion is mainly driven by the production of POF_3 and formaldehyde (OCH_2) gas species, it is only governed by the release of HF in the case of flaming combustion occurrence. By using equation (3) in the first approach, the time at which individuals may be expected to experience compromised tenability is assessed to be two time shorter in case of fire as compared to cell degassing

emission only.

More detailed analysis of the toxic threats potentially arising from batteries and affected by the studied influencing factors (combustion conditions, level of integration of electrically abused cell) such as those published by Diallo *et al* for ionic liquids or by Eshetu *et al* on battery electrolytes and their solvents[41,49,50] would be needed to confirm these preliminary results, in particular in case of cell chemistry changes. Although ISO 13571 standard is the state-of-the-art to address for the consequences of human exposure to the life incapacitation threat components of fire, significant limits persist in its operational use. Synergistic effects on top of additive effect of individual gas species as well as the effects of aerosols and particles and their interactions with emitted gases are not considered. Other organic species potentially present in the fumes such as organic carbonates and fluorinated organic species reported by Michel Armand and Stephane Laruelle[51,52] might affect overall toxicity and should be better examined from a toxicity point of view.

At module, pack and system levels, the presence of extra materials (plastics, wires…) can also contribute to the production of toxic gases (HF, HCl, HBr, CO…). Depending on the application, this external source of gas might even become predominant.

The presence of metallic elements (Ni, Co, Mn, Al, Li) in particulate emissions and fluoride ions in the fumes might also play a role in toxicity and further studies are needed in this domain, since current toxicity knowledge of fire smoke aerosols is essentially relevant to the combustion of conventional fuels burning, hydrocarbon materials and essentially emitting soot. In addition to those particles present in the fumes, battery thermal runaway also produces fragments not swept along with fumes[53] and might participate in the overall toxic hazard.

Explosion hazard (Atex formation)

The hazard brought by gas does not only result in its toxicity threat. Some gases are liable to create an Explosive Atmosphere (Atex) that might be of a great concern in poorly ventilated underground parking-lot or any confined space were batteries are present. For instance, explosions have been reported in several recent accidents[11,13]. In the emitted gas, the species known to form explosive gas mix are CH_4 , C_2H_4 CO, carbonates and H_2. These species are not present when the fire occurs in well ventilated conditions due to their good combustible properties, resulting in a much lower explosion hazard.

Soil/water pollution hazard

Incidents on large battery system can require the use of large amounts of water[10]. If the soil is not well protected, soot, unburned electrolyte leakage and particles can be carried along with extinction water and result in soil or water pollution. From this point of view, and notwithstanding the potential interaction with water, presence of flame might act as a negative factor since it increases particle emission even if it does not modify substantially the particles compositions.

Specific nature of particles as compared to (carbon based) soot emitted in conventional fires involving hydrocarbons and most combustible materials, would however require dedicated research to provide more consistent information regarding this aspect.

4. Conclusion

The influence of the developing scenario on the hazard produced in case of thermal runaway was studied, by mocking-up various levels of integration. Each level uses the same NMC cell to perform abuse tests. Tests carried out represented three cases: a) an isolated cell (not bound to any other neighboring cell), b) a cell inserted as the central cell in a cluster of three cells and subsequent additional parts (holder,…) and c) the same cell in the same cluster,

itself integrated as central cluster in a full module comprising three identical clusters, reflecting the 3 modularity layers of the mocked-up pack.

Our key results are as follow. The occurrence of flaming combustion events and their time of appearance and duration has shown to have a great impact on the resulting risk by modifying drastically the gas emission and the heat release profiles. Cell electrical abuse tests performed at different levels of cell integration, in consistency with battery pack usual modularity concept (cell or assembly of cells in clusters and modules) showed marked differences in behavior during thermal runaway, subsequently resulting in different hazards. This critical endpoint for adequate thermal runaway consideration in safety studies should be kept in mind when computing simulations using numerical models. Extrapolating abusive test results obtained at isolated cell level to anticipate behavior at higher levels of cell integration (module or pack) should be very carefully interpreted.

The detailed gas analysis performed during the different tests gave quantitative and qualitative insight in the gas production of a Li-ion cell at different levels (cell and cluster) during thermal runaway. It shows that the toxicity of the gas mix is affected by the presence or absence of outer flaming combustion. When no flaming combustion process is observed, significant CO production makes the gas entail a more asphyxiating character (according to calculated FED index) than when flaming combustion is developing. Consistently with fuel lean conventional fires, as compared to fuel rich ones[54], the battery thermal runaway reaction leads to a drastic increase in CO emission under low ventilation conditions. In contrast, because critical HF production is bound to fire development, tenability (FEC) is assessed to be twice as short as compared to thermal runaway ending up only by smoke degassing.

Fire (e.g. flaming combustion) is essentially fueled by flammable gases like H_2 and low molecular weight hydrocarbons or organic carbonates vapors. Flaming combustion therefore

prevents potential accumulation of flammable gas and avoids formation of an explosive atmosphere.

During the thermal runaway, the released heat has been quantified using CDG fire calorimetry and the corresponding thermal threat at a given distance from radiation by the use of heat fluxmeters. Our results show that when flaming combustion occurs, corresponding release of thermal energy increases rapidly and the risk of propagation to the adjacent cells becomes significant.

Last hazard considered in this study is particles emissions. Contrary to gas emissions the mix of particles emitted with or without fire development seems qualitatively similar (likely due to the same thermal decomposition processes taking place within the cells, essentially) and is produced in larger amount when fire starts.

When performing a comprehensive risk analysis of a battery system, other hazards that are out of the scope of this study should be taken into account, such as, electrolyte spilling, projection, electric arc formation, or corrosion issues. Moreover, potential confinement of a given battery energy storage system (as for instance in an electrical energy storage ISO container) might also modify fire and explosion risk in relation with flammable and toxic gas emissions that are not considered here.

Credit authorship contribution statement

Arnaud Bordes was involved in conceptualization, Investigation, formal analysis and in writing of the original manuscript; Guy Marlair was involved in supervision, validation, review and editing ; Aurélien Zantman was involved in investigation ; Sylvie Herreyre was involved in investigation; Arnaud Papin was involved in investigation ; Philippe Desprez was involved in project administration and Amandine Lecocq was involved in supervision, investigation, formal analysis and in writing of the original manuscript.

Declaration of competing interest

The authors declare that they have no known competing financial interest or personal relationships that could have appeared to influence the work reported in this paper.

Acknowledgments

This work was done in the scope of DEMOBASE project that has received funding from the European Union's Horizon 2020 research and innovation program under grant agreement Nr 769900**.** The funding organization was not involved in the drafting process of this paper.

Provision by RISE of FTIR calibration data regarding POF_3 compound is also gratefully acknowledged.

We are grateful to IFEVS for the delivery of test cell assemblies in clusters and module

References

1 Administration, U. S. E. I. Battery Strorage in the United States : An Update on Market Trends. (2020).

2 DNVGL. Recommended practice - DNVGL-RP-0043 - Safety, operation a,d performance of grid connected energy storage systems. (2017).

3 Walker, D. PAS 7060:2021Electric vehicles – Safe and environmentally-conscious design and use of batteries – Guide. (2021).

4 UNECE. https://unece.org/status-1958-agreement-and-annexed-regulations. *last acessed november 2021* (1958).

5 UNECE. https://unece.org/transport/dangerous-goods/un-model-regulations-rev-22. *late acess november 2021* (2021).

6 Chen, Y. *et al.* A review of lithium-ion battery safety concerns: The issues, strategies, and testing standards. *Journal of Energy Chemistry* (2020).

7 Ruiz, V. *et al.* A review of international abuse testing standards and regulations for lithium ion batteries in electric and hybrid electric vehicles. *Renewable and Sustainable Energy Reviews* **81**, 1427-1452 (2018).

8 Soares, F. J. *et al.* The STABALID project: Risk analysis of stationary Li-ion batteries for power system applications. *Reliability Engineering & System Safety* **140**, 142-175 (2015).

9 Bubbico, R., Greco, V. & Menale, C. Hazardous scenarios identification for Li-ion secondary batteries. *Safety science* **108**, 72-88 (2018).

10 Christensen, P. A. *et al.* Risk management over the life cycle of lithium-ion batteries in electric vehicles. *Renewable and Sustainable Energy Reviews* **148**, 111240 (2021).

11 Hill, D. McMicken Battery Energy Storage System Event Technical Analysis and Recommendations. *DNV.GL* (2020).

12 Zalosh, R., Gandhi, P. & Barowy, A. Lithium-ion energy storage battery explosion incidents. *Journal of Loss Prevention in the Process Industries*, 104560 (2021).

13 Sun, P., Bisschop, R., Niu, H. & Huang, X. A review of battery fires in electric vehicles. *Fire technology*, 1-50 (2020).

14 CTIF. Accident analysis of Beijing Jimei Dahongmen 25 MWh DC solar-storage-charging integrated station project. *https://www.ctif.org/news/accident-analysis-beijing-lithium-battery-explosion-which-killed-two-firefighters* **last accessed Septembrer 2021** (2021).

15 Sturk, D., Rosell, L., Blomqvist, P. & Ahlberg Tidblad, A. Analysis of li-ion battery gases vented in an inert atmosphere thermal test chamber. *Batteries* **5**, 61 (2019).

16 Baird, A. R., Archibald, E. J., Marr, K. C. & Ezekoye, O. A. Explosion hazards from lithium-ion battery vent gas. *Journal of Power Sources* **446**, 227257 (2020).

17 Kong, W., Li, H., Huang, X. & Chen, L. Gas evolution behaviors for several cathode materials in lithium-ion batteries. *Journal of power sources* **142**, 285-291 (2005).

18 Ribière, P. *et al.* Investigation on the fire-induced hazards of Li-ion battery cells by fire calorimetry. *Energy & Environmental Science* **5**, 5271-5280 (2012).

19 Maloney, T. Lithium Battery Thermal Runaway Vent Gas Analysis Composition and Effect of Combustion. *Federal Aviation Administration* (2016).

20 Jiang, F., Liu, K., Wang, Z., Tong, X. & Guo, L. Theoretical analysis of lithium-ion battery failure characteristics under different states of charge. *Fire and Materials* **42**, 680-686 (2018).

21 Tanim, T. R., Dufek, E. J. & Sazhin, S. V. Challenges and needs for system-level electrochemical lithium-ion battery management and diagnostics. *MRS Bulletin*, 1-9 (2021).

22 Li, W. *et al.* Fire boundaries of lithium-ion cell eruption gases caused by thermal runaway. *Iscience* **24**, 102401 (2021).

23 https://www.demobase-project.eu/. https://www.demobase-project.eu/. *last accessed september 2021* (2021).

24 Petit, M. *et al.* in *Proceedings of the 32nd Electric Vehicle Symposium (EVS32), Lyon, France.*

25 Bordes, A. *et al.* A holistic contribution to fast innovation in electric vehicles: An overview of the DEMOBASE research project. *eTransportation*, 100144 (2021).
26 Zhang, G. *et al.* Internal short circuit mechanisms, experimental approaches and detection methods of lithium-ion batteries for electric vehicles: A review. *Renewable and Sustainable Energy Reviews* **141**, 110790 (2021).
27 ISO 19702:2006 : Toxicity testing of fire effluents - Guidance for analysis of gases and vapours in fire effluents using FTIR gas analysis. (2006).
28 Pretrel, H., Le Saux, W. & Audouin, L. Experimental determination of fire heat release rate with OC and CDG calorimetry for ventilated compartments fire scenario. *Fire and Materials* **38**, 474-506 (2014).
29 Biteau, H., Fuentes, A., Marlair, G., Brohez, S. & Torero, J. L. Ability of the Fire Propagation Apparatus to characterise the heat release rate of energetic materials. *Journal of hazardous materials* **166**, 916-924 (2009).
30 Brohez, S., Delvosalle, C., Marlair, G. & Tewarson, A. in *Proceedings of the 13th International Congress of Chemical and Process Engineering (2nd Symposium on Environmental and Safety Engineering, CHISA 98), paper.* 12 (Citeseer).
31 Bryant, R. & Bundy, M. The NIST 20 MW calorimetry measurement system for large-fire research (NIST technical note TN 2077). *Gaithersburg, MD: National Institute of Standards and Technology* (2019).
32 Lyon, R. E. & Walters, R. N. Energetics of lithium ion battery failure. *Journal of Hazardous Materials* **318**, 164-172, doi:https://doi.org/10.1016/j.jhazmat.2016.06.047 (2016).
33 Truchot, B., Fouillen, F. & Collet, S. An experimental evaluation of toxic gas emissions from vehicle fires. *Fire safety journal* **97**, 111-118 (2018).
34 Fernandes, Y., Bry, A. & de Persis, S. Thermal degradation analyses of carbonate solvents used in Li-ion batteries. *Journal of Power Sources* **414**, 250-261 (2019).
35 Larsson, F., Andersson, P., Blomqvist, P. & Mellander, B.-E. Toxic fluoride gas emissions from lithium-ion battery fires. *Scientific reports* **7**, 1-13 (2017).
36 Larsson, F., Andersson, P., Blomqvist, P., Lorén, A. & Mellander, B.-E. Characteristics of lithium-ion batteries during fire tests. *Journal of Power Sources* **271**, 414-420 (2014).
37 Yuan, L., Dubaniewicz, T., Zlochower, I., Thomas, R. & Rayyan, N. Experimental study on thermal runaway and vented gases of lithium-ion cells. *Process Safety and Environmental Protection* **144**, 186-192 (2020).
38 Tsuchiya, Y. CO/CO2 ratios in fire. *Fire Safety Science* **4**, 515-526 (1994).
39 ISO 19706:2011 : Guidelines for assessing the fire threat to people. (2011).
40 Solchenbach, S., Metzger, M., Egawa, M., Beyer, H. & Gasteiger, H. A. Quantification of PF5 and POF3 from side reactions of LiPF6 in Li-ion batteries. *Journal of The Electrochemical Society* **165**, A3022 (2018).
41 Eshetu, G. G. *et al.* Fire behavior of carbonates-based electrolytes used in Li-ion rechargeable batteries with a focus on the role of the LiPF6 and LiFSI salts. *Journal of Power Sources* **269**, 804-811 (2014).
42 Forestier, C. *et al.* Study of the Role of LiNi1/3Mn1/3Co1/3O2/Graphite Li-Ion Pouch Cells Confinement, Electrolyte Composition and Separator Coating on Thermal Runaway and Off-Gas Toxicity. *Journal of The Electrochemical Society* **167**, 090513 (2020).
43 INRS ND 2097-174-99 Thermal degradation of Plastics. (1999).
44 De Soete, G. Mécanismes physico-chimiques de formation et de réduction de NOx dans les flammes d'hydrocarbures. *Revue de l'Institut Français du Pétrole* **33**, 747-792 (1978).
45 Ola Willstrand, R. B., Per Blomqvist, Alastair Temple, Johan Anderson. Toxic Gases from Electric Vehicle Fires. *electronic proceedings FIVE2020 conference, https://www.ri.se/sites/default/files/2020-12/FIVE2020_Willstrand.pdf last accessed november 2021* (2020).
46 Janssens, M. in *SFPE Handbook of Fire Protection Engineering* 905-951 (Springer, 2016).

47 Quintiere, J. On methods to measure the energetics of a lithium ion battery in thermal runaway. *Fire safety journal* **111**, 102911 (2020).
48 ISO 13571:2012 Life-threatening components of fire — Guidelines for the estimation of time to compromised tenability in fires. (2012).
49 Morgan, A. B., Len, C. & Marlair, G. An innovative experimental approach aiming to understand and quantify the actual fire hazards of ionic liquids. *Energy & Environmental Science* **6**, 699-710 (2013).
50 Diallo, A., Truchot, B., Marlair, G. & Len, C. An Insight of Combustibility Induced Safety Issues Pertaining to Ionic Liquids.
51 Hammami, A., Raymond, N. & Armand, M. Runaway risk of forming toxic compounds. *Nature* **424**, 635-636 (2003).
52 Gachot, G. *et al.* Deciphering the multi-step degradation mechanisms of carbonate-based electrolyte in Li batteries. *Journal of Power Sources* **178**, 409-421 (2008).
53 Zhang, Y., Wang, H., Li, W., Li, C. & Ouyang, M. Size distribution and elemental composition of vent particles from abused prismatic Ni-rich automotive lithium-ion batteries. *Journal of Energy Storage* **26**, 100991 (2019).
54 Brohez, S., Marlair, G. & Delvosalle, C. The effect of oxygen concentration on CO and soot yields in fires. *Fire and Materials: An International Journal* **32**, 141-158 (2008).